Highly sensitive CO_2-LITES sensor based on a self-designed low-frequency quartz tuning fork and fiber-coupled MPC

Jinfeng Hou (侯金凤), Xiaonan Liu (刘晓楠), Yahui Liu (刘亚辉), Ying He (何应), Weijiang Zhao (赵卫疆), and Yufei Ma (马欲飞)*

National Key Laboratory of Science and Technology on Tunable Laser, Harbin Institute of Technology, Harbin 150001, China

** Corresponding author: E-mail: mayufei@hit.edu.cn*

Received Month X, XXXX; accepted Month X, XXXX; posted online Month X, XXXX

A highly sensitive carbon dioxide (CO_2) sensor based on light-induced thermoelastic spectroscopy (LITES) utilizing a self-designed low-frequency quartz tuning fork (QTF) and a fiber-coupled multipass cell (MPC) is reported in this paper. The QTF with low resonant frequency of 8675 Hz and high Q factor of 11675.64 was used to improve its energy accumulation time and the sensor's signal level. The MPC with fiber-coupled structure and optical length of 40 m was adopted to significantly increase the gas absorbance and reduce the optical alignment difficulty as well as improve the robustness of the sensor system. A distributed feedback (DFB), near-infrared diode laser with emission wavelength of 1.57 μm was used as an excitation source. The experimental results showed that this CO_2-LITES sensor had excellent linear response to CO_2 concentrations. The minimum detection limitation (MDL) of this CO_2-LITES sensor was obtained to be 445.91 ppm and it can be improved to 47.70 ppm when the integration time of the system reached 500 s. Further improvement methods for detection performance of such sensor were discussed.

Keywords: *carbon dioxide (CO_2), quartz tuning fork (QTF), multipass cell, light -induced thermoelastic spectroscopy (LITES)*

DOI: 10.3788/COLXXXXXX.XXXXXX

1. Introduction

Carbon dioxide (CO_2) is one of the major greenhouse gases in the atmosphere. Fossil fuels [1], automobile exhaust [2], and industrial emissions [3] are the main sources of CO_2. Increasing concentrations of CO_2 can lead to global warming and various environmental problems [4], so the detection of CO_2 concentration is of great significance in air pollutant monitoring. In healthcare, the detection of CO_2 concentration contributes to prevent and treat respiratory diseases [5]. CO_2 detection also plays an important role in the field of agriculture, where the state of seeds can be determined by detecting the concentration of CO_2 produced by the seeds [6]. Therefore, the development of CO_2 gas sensors with high sensitivity is essential.

So far, many types of CO_2 sensors including electrochemical sensors [7], semiconductor sensors [8] and optical sensors [9] have been developed. Among them, the most attractive is laser spectroscopy based detection technique, which is employed because of its high sensitivity, fast response and high specificity [10-26]. In 2002, Tittel et al. proposed the quartz-enhanced photoacoustic spectroscopy (QEPAS) [27], in which a quartz tuning fork (QTF) is used as an acoustic detector instead of the traditional microphone. The benefits of QEPAS over conventional photoacoustic spectroscopy include its small size and strong interference immunity [28-35]. However, QEPAS requires that the QTF must be placed in the environment of the gas to be measured, which means that QEPAS cannot perform non-contact measurements [36-38], resulting in application limitations. Furthermore, QEPAS technique can't be used to detect corrosive gases, and to detect gas at high temperatures because the QTF will be oxidized or damaged in these cases [39,40].

To address the shortcomings of QEPAS mentioned above, Ma et al. first proposed light-induced thermoelastic spectroscopy (LITES) in 2018 [41]. In this technique, the laser light will be absorbed partly after passing through the gas to be measured, and the remaining light is irradiated at the root of the QTF, which makes the heat distribution on the surface of the QTF uneven. Due to the light-induced thermoelastic effect [42], the QTF generates a mechanical vibration, and the vibration is enhanced when the modulation frequency of the laser is the same as the resonant frequency of the QTF [43]. Ultimately, the vibration is transformed into an electrical signal via the piezoelectric effect. Demodulation this electrical signal can reverse the gas concentration [44,45]. LITES is a good solution to the shortcomings of QEPAS, as the QTF does not need to be in contact with the gas to be measured, realizing non-contact measurements. Till now, various gases detection based on LITES have been reported [46-54].

QTF, as the detection unit of the LITES technology, has a significant impact on the performance of the system [55]. So far, the most commonly used QTF is the commercial available one with a resonant frequency of 32.768 kHz. However, the performance of QTF is related to the energy accumulation time [56]. The higher the resonant frequency of the QTF, the shorter the energy accumulation time of the QTF, resulting in poor detection sensitivity. From 2014, Spagnolo et al. carried out a study on the optimal design of QTF [57,58]. By optimizing the size and shape, a low-frequency QTF can be obtained [59], which can significantly increase the sensor system's sensitivity by serving as the detection unit in LITES technique.

Apart from QTFs, another crucial component of the LITES system is multipass cell (MPC), which is used to enhance the optical absorption. The commonly used MPC is composed of two concave mirrors with high reflectivity, and the laser beam is incident at a specific angle into the

MPC, which is reflected between the two concave mirrors

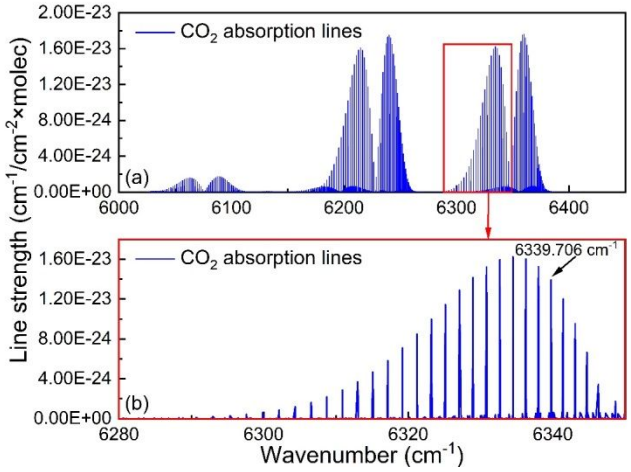

Fig. 1 Simulation of CO_2 absorption based on the HITRAN 2023 database. (a) CO_2 absorption line intensity in the range of 6000-6450 cm^{-1}; (b) CO_2 absorption line located at 6339.706 cm^{-1}.

several times and then ejected from the light outlet. Only when the MPC is incident at the proper angle will it have the necessary effective length. Therefore, this type of MPC has the disadvantage of being difficult to align optically [60], and the inclusion of many optical components in the optical alignment makes the sensor system unstable. Thus, in order to eliminate the shortcomings of the widely used MPC, this study presents a fiber-coupled MPC, in which the interior of the MPC is identical to that of the conventional MPC and the laser beam is incident into the MPC through an optical fiber and then out through another optical fiber. This design solves the problem of difficult optical alignment of the conventional MPC and improves the stability of the sensor system.

In this paper, a high sensitive CO_2-LITES sensor based on a self-designed low-frequency QTF and fiber-coupled MPC was reported for the first time. The low resonant frequency of 8.7 kHz is beneficial to improve the signal level. A fiber-coupled MPC with an optical length of 40 m was employed, which significantly increased the gas absorption and also reduced the optical alignment difficulty and improved the robustness of the system. To eliminate the background noise, wavelength modulation spectroscopy (WMS) and the second harmonic (2*f*) signal demodulation were applied. The Allan deviation was used to assess the system's long-term stability.

2. Experimental setup

2.1 Selecting the CO_2 absorption line

Based on the HITRAN2023 database, the CO_2 absorption line intensity in the range of 6000-6450 cm^{-1} is shown in Fig. 1(a). This range of light interacts well with optical fibers with low loss, and is easily transferred via an all-fiber system. Due to the tuning ability of the used diode laser, the line at 6339.706 cm^{-1} (1577.36 nm) was chosen as the target absorption line in order to achieve good detection performance, which is shown in Fig. 1(b).

The sensor utilized a distributed feedback (DFB) diode laser with an emission wavelength of 1.57 μm. The variation of the laser output wavelength with injected current at different operating temperatures can be found in Fig. 2(a). The relationship between the laser output power and injected current at different operating temperatures is displayed in Fig. 2(b). It is discovered that when the injected current increased, the laser's output power and wavelength rose as well. The maximum output power of 20.33 mW was achieved when the current was 140 mA.

2.2 The schematic diagram of experimental setup

Fig. 3 shows the CO_2-LITES sensor's experimental setup. The beam emitting from the pigtail of the DFB diode laser entered the fiber-coupled MPC through a fiber optic connector, and the beam left from the exit port following several reflections in the MPC. The light travelled through the fiber collimator (FC) and lens before focusing on the root of the self-designed QTF, where the strongest LITES signal is produced. The image of the used QTF is shown in Fig. 3(a). The length of a normal QTF is about 0.5 cm, but the self-designed QTF is four times longer than it and the top of the self-designed QTF finger is trapezoidal for increasing the sensitivity. In this work background noise was

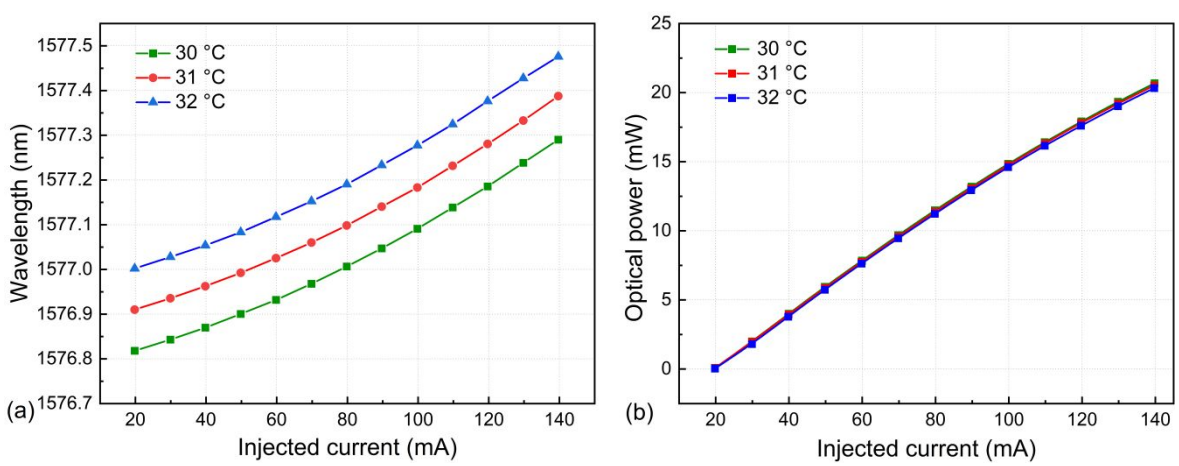

Fig. 2 Laser characteristics. (a) The relationship between the output wavelength and injected current at different temperatures; (b) The relationship between the output power and injected current different temperatures.

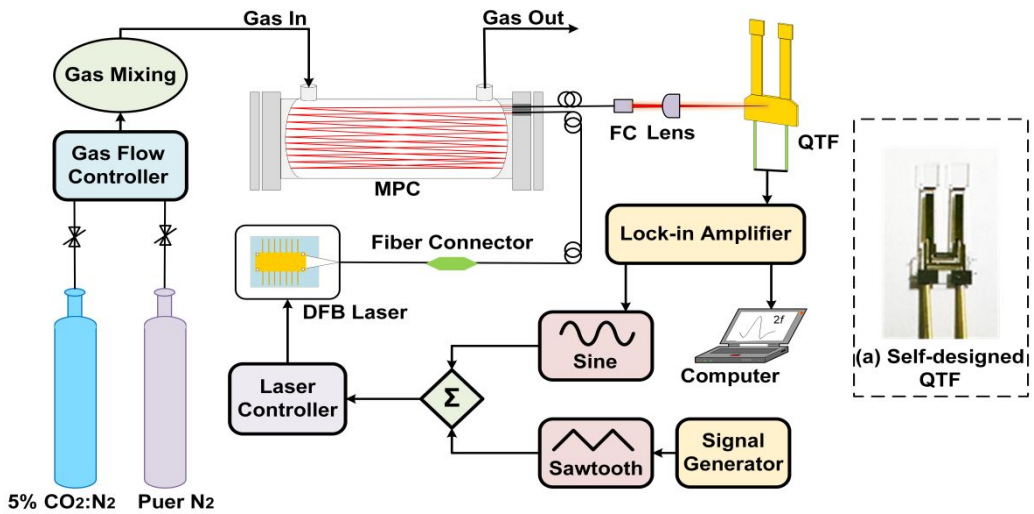

Fig. 3. The schematic diagram of the CO_2-LITES sensor.

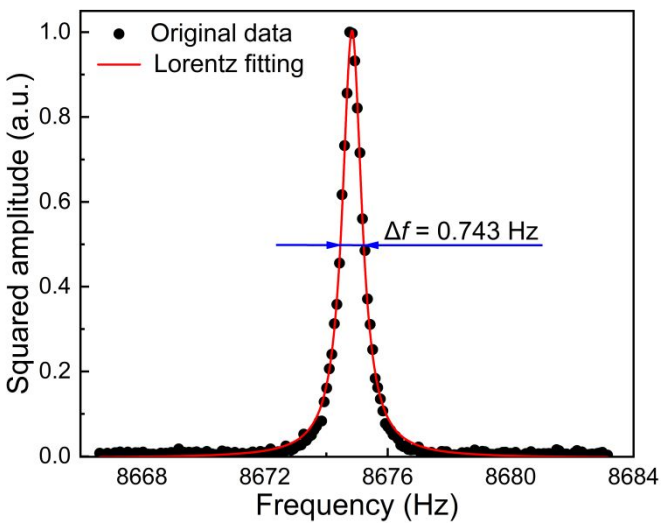

Fig. 4 The frequency response of the self-designed QTF

decreased by using a wavelength modulation spectroscopy (WMS) approach based on the second harmonic (2*f*) detection. The CO_2 target absorption line was scanned by a triangle wave produced by a signal generator, while a sine wave produced by the lock-in amplifier was used for wavelength modulation. An adder superimposed the sine and triangular waves and fed them into the laser controller to control laser parameter. A lock-in amplifier demodulated and examined the 2f signal produced by the QTF, and its integration time and detection bandwidth were 200 ms and 0.08 Hz. The laser used in this work had a TEC temperature of 32 °C and a scanning current range from 70 to 130 mA. Different CO_2 concentrations were achieved by combining 5% CO_2 with pure nitrogen (N_2). A mass flow meter was used to control the flow rate at 300 mL/min.

3. Experimental results and discussions

Firstly, the optical excitation method was used to evaluate the frequency response (f_0) of the QTF. The QTF frequency response curve is displayed in Fig. 4, which has been normalized and Lorentz fitted. The QTF has a f_0 of 8675 Hz and bandwidth Δf of 0.743 Hz. According to the equation $Q = f_0/\Delta f$, the Q-factor was calculated as 11675.64, indicating the self-designed QTF has a long energy accumulation time.

The modulation depth is an important parameter in second harmonic detection, and the 2*f* signal amplitude has a close connection with the modulation depth. Fig. 5 illustrates the relationship between the 2*f* signal amplitude of CO_2-LITES sensor and the laser current modulation depth. It is evident that with the increase of the modulation current, the amplitude of the 2*f* signal firstly increased and then flattened out. Comprehensive considering the laser parameters and experimental requirements, the modulation depth of 22 mA is selected in the following experiments.

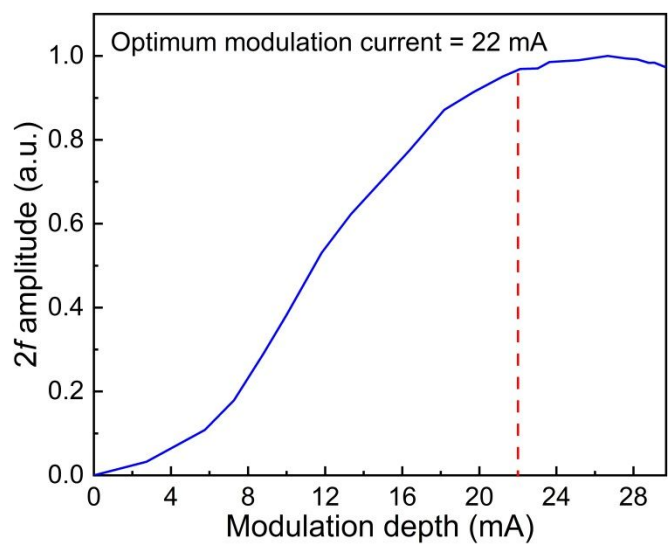

Fig. 5 The variation trend between the 2*f* signal amplitude and current modulation depth

To investigate the linear response of the sensor to CO_2 concentration, 2*f* signals at different CO_2 concentrations were collected, and the results are displayed in Fig. 6(a).

The relationship between the 2*f* signal amplitude and CO_2

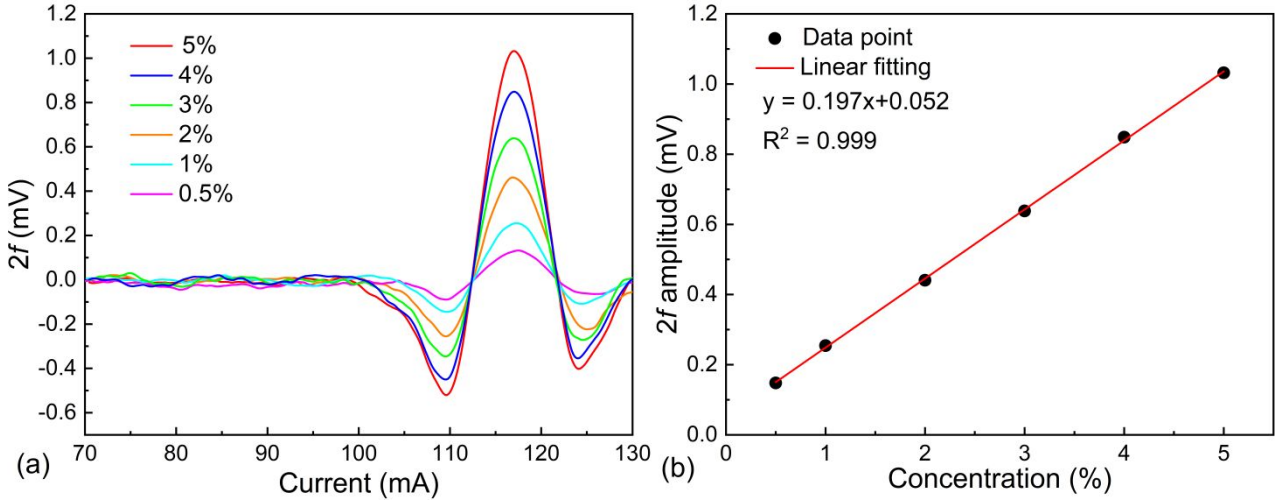

Fig. 6 Relationship between the 2*f* signal and CO_2 concentration. (a) The 2*f* signal under different CO_2 concentrations; (b) The peak value of 2*f* signal at various CO_2 concentrations and the associated linear fitting

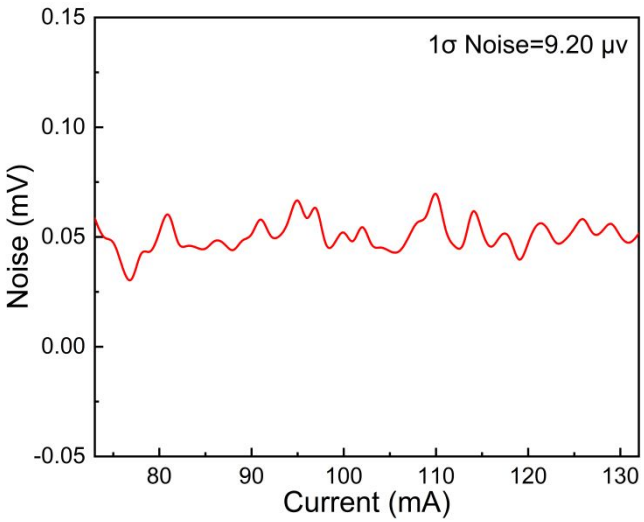

Fig. 7 Noise determination of CO_2-LITES sensor

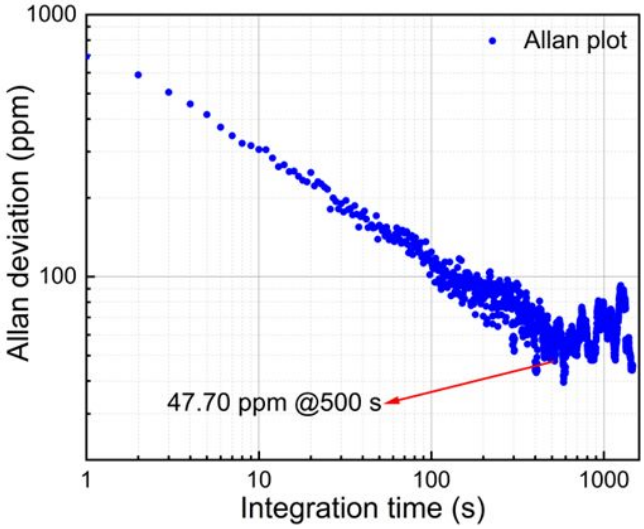

Fig. 8 Allan deviation analysis of CO_2-LITES sensor

concentration is shown in Fig. 6(b). The calculated R-squared value was 0.999, which indicated that this CO_2-LITES sensor had an excellent linear response for CO_2 concentration detection.

Under the condition that the MPC was filled with pure N_2, the measured noise is displayed in Fig. 7 with a 1 σ noise value of 9.20 μV. Therefore, under the condition that the CO_2 concentration was 5%, the signal-to-noise ratio (SNR) was calculated to be 112.13. Dividing the concentration by the SNR yielded the minimum detection limitation (MDL), which is calculated to be 445.91 ppm.

In order to obtain the stability of the CO_2-LITES sensor system and its optimal detection capability, continuous monitoring was performed for 2.5 hours when the MPC was filled with pure N_2. Fig. 8 displays the Allan deviation analysis performed on the experimental data. The MDL reached 47.70 ppm when the integration time was 500 s, which proved that the reported CO_2-LITES sensor had good stability.

4. Conclusion

In this paper, a high sensitive CO_2-LITES sensor based on a self-designed QTF and a fiber-coupled MPC was reported for the first time. The resonant frequency of 8.765 kHz and Q factor of 11675.64 of the used QTF are advantageous to improve the energy accumulation time and the sensor's signal level. The MPC with fiber-coupled structure and optical length of 40 m significantly increases the gas absorption and reduces the optical alignment difficulty as well as improves the robustness of the sensor system. Targeting the CO_2 absorption line at 1576.94 nm, a near-infrared DFB diode laser with an output power of 16.9 mW was used as the excitation source. The experimental results showed that this CO_2-LITES sensor had excellent linear response to CO_2 concentrations. A MDL of 47.70 ppm was obtained when the integration time reached 500 s, indicating such CO_2-LITES sensor had outstanding system stability. The sensor performance can be further improved when a strong absorption line located at 2 μm or mid-infrared region is adopted [61,62].

Acknowledgments

We are grateful for financial supports from the National Natural Science Foundation of China (Grant No. 62335006, 62022032 and 62275065), Key Laboratory of Opto-Electronic Information Acquisition and Manipulation (Anhui University), Ministry of Education (Grant No. OEIAM202202), Fundamental Research Funds for the Central Universities (Grant No. HIT.OCEF.2023011).

References

1. A. G. Olabi and M. A. Abdelkareem, "Renewable energy and climate change," Renew. Sust. Energ. Rev. **158**, 112111 (2022).
2. R. Kawamoto, H. Mochizuki, Y. Moriguchi, T. Nakano, M. Motohashi, Y. Sakai, and A. Inaba, "Estimation of CO_2 emissions of internal combustion engine vehicle and battery electric vehicle using LCA," Sustainability **11**, 2690 (2019).
3. H. Xu, Y. Ge, C. Zhang, Z. Wang, B. Xu, H. Zhao, J. Huang, G. Wang, J. Liu, Y. Feng, and G. Shi, "Machine learning reveals the effects of drivers on PM2.5 and CO_2 based on ensemble source apportionment method," Atmos. Res. **295**, 107019 (2023).
4. E. A. G. Schuur, A. D. McGuire, C. Schaedel, G. Grosse, J. W. Harden, D. J. Hayes, G. Hugelius, C. D. Koven, P. Kuhry, D. M. Lawrence, S. M. Natali, D. Olefeldt, V. E. Romanovsky, K. Schaefer, M. R. Turetsky, C. C. Treat, and J. E. Vonk, "Climate change and the permafrost carbon feedback," Nature **520**, 171 (2015).
5. G. D'Amato, H. J. Chong-Neto, O. P. Monge Ortega, C. Vitale, I. Ansotegui, N. Rosario, T. Haathela, C. Galan, R. Pawankar, M. Murrieta, L. Cecchi, C. Bergmann, E. Ridolo, G. Ramon, S. G. Diaz, M. D'Amato, and I. Annesi-Maesano, "The effects of climate change on respiratory allergy and asthma induced by pollen and mold allergens," Allergy **75**, 2219 (2020).
6. L. Gao, Y. Zang, G. Zhao, H. Qi, Q. Tang, Q. Liu, and L. Jia, "Research on the seed respiration CO_2 detection system based on TDLAS technology," Int. J. Opt. **2023**, 8017726 (2023).
7. A. Hannon and J. Li, "Solid state electronic sensors for detection of carbon dioxide," Sensors **19**, 3848 (2019).
8. B. Ersoez, K. Schmitt, and J. Woellenstein, "CO_2 gas sensing with an electrolyte-gated transistor using impedance spectroscopy," Sens. Actuators B Chem. **334**, 129598 (2021).
9. T. He, W. Wang, B.-G. He, and J. Chen, "Review on optical fiber sensors for hazardous-gas monitoring in mines and tunnels," IEEE Trans. Instrum. Meas. **72**, 7003722 (2023).
10. J. Le, Y. Su, C. Tian, A.H. Kung, Y. Ron Shen, "A novel scheme for ultrashort terahertz pulse generation over a gapless wide spectral range: Raman-resonance-enhanced four-wave mixing," Light Sci. Appl. **12**, 34 (2023).
11. Y. Liu, S. Qiao, C. Fang, Y. He, H. Sun, J. Liu, and Y. Ma, "A highly sensitive LITES sensor based on a multi-pass cell with dense spot pattern and a novel quartz tuning fork with low frequency," Opto-Electron. Adv. **7**, 230230 (2024).
12. K. Hashimoto, T. Nakamura, T. Kageyama, V. R. Badarla, H. Shimada, R. Horisaki, and T. Ideguchi, "Upconversion time-stretch infrared spectroscopy," Light Sci. Appl. **12**, 48 (2023).
13. J. Chen, T. Eul, L. Lyu, Y. Li, X. Hu, X. Ning, S. Wang, M. Aeschlimann, Q. Gong, "Tracing the formation of oxygen vacancies at the conductive $LaAlO_3/SrTiO_3$ interface via photoemission," Opto-Electron. Sci. **1**, 210011 (2022).
14. P. P. Shum, G. Keiser, G. Humbert, D. J. J. Hu, A. P. Zhang, and L. Su, "Highly sensitive microfiber ultrasound sensor for photoacoustic imaging," Opto-Electron. Adv. **6**, 230065 (2023).
15. W. Yang, F. Knorr, I. Latka, M. Vogt, GO. Hofmann, J. Popp, IW. Schie. "Real-time molecular imaging of near-surface tissue using Raman spectroscopy," Light Sci. Appl. **11,** 90 (2022).
16. S. Jiang, F. Chen, Y. Zhao, S. Gao, Y. Wang, H. L. Ho, and W. Jin, "Broadband all-fiber optical phase modulator based on photo-thermal effect in a gas-filled hollow-core fiber," Opto-Electron. Adv. **6**, 220085 (2023).
17. C. Zhang, S. Qiao, Y. He, and Y. Ma, "Trace gas sensor based on a multi-pass-retro-reflection-enhanced differential Helmholtz photoacoustic cell and a power amplified diode laser," Opt. Express **32**, 848 (2024).
18. Z. Zhang, T. Peng, X. Nie, G. S. Agarwal, and M. O. Scully, "Entangled photons enabled time-frequency-resolved coherent Raman spectroscopy and applications to electronic coherences at femtosecond scale," Light Sci. Appl. **11**, 274 (2022).
19. X. Wang, X. Qiu, M. Liu, F. Liu, M. Li, L. Xue, B. Chen, M. Zhang, P. Xie, "Flat soliton microcomb source," Opto-Electron. Sci. **2**, 230024 (2023).
20. C. Zhang, Y. He, S. Qiao, and Y. Ma, "Differential integrating sphere-based photoacoustic spectroscopy gas sensing," Opt. Lett. **48**, 5089 (2023).
21. M. Shao, C. Ji, J. Tan, B. Du, X. Zhao, J. Yu, B. Man, K. Xu, C. Zhang, and Z. Li, "Ferroelectrically modulate the Fermi level of graphene oxide to enhance SERS response," Opto-Electron. Adv. **6**, 230094 (2023).
22. Z. Zheng, S. Zhu, Y. Chen, H. Chen, J. Chen, "Towards integrated mode-division demultiplexing spectrometer by deep learning," Opto-Electron. Sci. **1**, 220012 (2022).
23. Y. Wang, H. Du, Y. Li, F. Mei, Y. Hu, L. Xiao, J. Ma, and S. Jia, "Testing universality of Feynman-Tan relation in interacting Bose gases using high-order Bragg spectra," Light Sci. Appl. **12**, 50 (2023).
24. W. Chen, S. Qiao, Z. Zhao, S. Gao, Y. Wang, and Y. Ma, "Sensitive carbon monoxide detection based on laser absorption spectroscopy with hollow-core antiresonant fiber," Microw. Opt. Techn. Lett. **66**, e33780 (2024).
25. H. Gao, X. Fan, Y. Wang, Y. Liu, X. Wang, K. Xu, L. Deng, C. Zeng, T. Li, J. Xia, W. Xiong, "Multi-foci metalens for spectra and polarization ellipticity recognition and reconstruction," Opto-Electron. Sci. **2**, 220026 (2023).
26. F. Wan, R. Wang, H. Ge, W. Kong, H. Sun, H. Wu, G. Zhao, W. Ma, and W. Chen, "Optical feedback frequency locking: impact of directly reflected field and responding strategies," Opt. Express 2024, doi: 10.1364/OE.520346.
27. A. A. Kosterev, Y. A. Bakhirkin, R. F. Curl, and F. K. Tittel, "Quartz-enhanced photoacoustic spectroscopy,"

Opt. Lett. **27**, 1902 (2002).
28. B. Sun, P. Patimisco, A. Sampaolo, A. Zifarelli, V. Spagnolo, H. Wu, and L. Dong, "Light-induced thermoelastic sensor for ppb-level H_2S detection in a SF_6 gas matrices exploiting a mini-multi-pass cell and quartz tuning fork photodetector," Photoacoustics **33**, 100553 (2023).
29. T. Liang, S. Qiao, Y. Chen, Y. He, and Y. Ma, "High-sensitivity methane detection based on QEPAS and H-QEPAS technologies combined with a self-designed 8.7 kHz quartz tuning fork," Photoacoustics **36**, 100592 (2024).
30. C. Zhang, S. Qiao, Y. He, S. Zhou, L. Qi, and Y. Ma, "Differential quartz-enhanced photoacoustic spectroscopy," Appl. Phys. Lett. **122**, 241103 (2023).
31. H. Lin, H. Zheng, B. A. Z. Montano, H. Wu, M. Giglio, A. Sampaolo, P. Patimisco, W. Zhu, Y. Zhong, L. Dong, R. Kan, J. Yu, and V. Spagnolo, "Ppb-level gas detection using on-beam quartz-enhanced photoacoustic spectroscopy based on a 28 kHz tuning fork," Photoacoustics **25**, 100321 (2022).
32. Y. Zhang, Y. Xie, J. Lu, J. Zhao, Y. Wu, J. Tong, and J. Shao, "Continuous real-time monitoring of carbon dioxide emitted from human skin by quartz-enhanced photoacoustic spectroscopy," Photoacoustics **30**, 100488 (2023).
33. G. Menduni, A. Zifarelli, A. Sampaolo, P. Patimisco, M. Giglio, N. Amoroso, H. Wu, L. Dong, R. Bellotti, and V. Spagnolo, "High-concentration methane and ethane QEPAS detection employing partial least squares regression to filter out energy relaxation dependence on gas matrix composition," Photoacoustics **26**, 100349 (2022).
34. C. Fang, T. Liang, S. Qiao, Y. He, Z. Shen, and Y. Ma, "Quartz-enhanced photoacoustic spectroscopy sensing using trapezoidal- and round-head quartz tuning forks," Opt. Lett. **49**, 770 (2024).
35. Z. Lang, S. Qiao, T. Liang, Y. He, L. Qi, and Y. Ma, "Dual-frequency modulated heterodyne quartz-enhanced photoacoustic spectroscopy," Opt. Express **32**, 379 (2024).
36. Y. Ma, Y. He, X. Yu, C. Chen, R. Sun, and F. K. Tittel, "HCl ppb-level detection based on QEPAS sensor using a low resonance frequency quartz tuning fork," Sens. Actuators B Chem. **233**, 388 (2016).
37. P. Patimisco, A. Sampaolo, L. Dong, F. K. Tittel, and V. Spagnolo, "Recent advances in quartz enhanced photoacoustic sensing," Appl. Phys. Rev. **5**, 011106 (2018).
38. W. Chen, S. Qiao, Y. He, J. Zhu, K. Wang, L. Qi, S. Zhou, L. Xiao, and Y. Ma, "Mid-infrared all-fiber light-induced thermoelastic spectroscopy sensor based on hollow-core anti-resonant fiber," Photoacoustics **36**, 100594 (2024).
39. H. Yi, R. Maamary, X. Gao, M. W. Sigrist, E. Fertein, and W. Chen, "Short-lived species detection of nitrous acid by external-cavity quantum cascade laser based quartz-enhanced photoacoustic absorption spectroscopy," Appl. Phys. Lett. **106**, 101109 (2015).
40. X. Liu and Y. Ma, "New temperature measurement method based on light-induced thermoelastic spectroscopy," Opt. Lett. **48**, 5687 (2023).
41. Y. Ma, Y. He, Y. Tong, X. Yu, and F. K. Tittel, "Quartz-tuning-fork enhanced photothermal spectroscopy for ultra-high sensitive trace gas detection," Opt. Express **26**, 32103 (2018).
42. Y. Ma, Y. He, P. Patimisco, A. Sampaolo, S. Qiao, X. Yu, F. K. Tittel, and V. Spagnolo, "Ultra-high sensitive trace gas detection based on light-induced thermoelastic spectroscopy and a custom quartz tuning fork," Appl. Phys. Lett. **116**, 011103 (2020).
43. C. Lou, X. Li, H. Chen, X. Yang, Y. Zhang, J. Yao, and X. Liu, "Polymer-coated quartz tuning fork for enhancing the sensitivity of laser-induced thermoelastic spectroscopy," Opt. Express **29**, 12195 (2021).
44. Y. Ma, Y. Hu, S. Qiao, Z. Lang, X. Liu, Y. He, and V. Spagnolo, "Quartz tuning forks resonance frequency matching for laser spectroscopy sensing," Photoacoustics **25**, 100329 (2022).
45. L. Hu, C. Zheng, M. Zhang, K. Zheng, J. Zheng, Z. Song, X. Li, Y. Zhang, Y. Wang, and F. K. Tittel, "Long-distance in-situ methane detection using near-infrared light-induced thermo-elastic spectroscopy," Photoacoustics **21**, 100230 (2021).
46. Z. Lang, S. Qiao, and Y. Ma, "Fabry–Perot-based phase demodulation of heterodyne light-induced thermoelastic spectroscopy," Light Adv. Manuf. **4**, 23 (2023).
47. C. Lou, X. Yang, X. Li, H. Chen, C. Chang, and X. Liu, "Graphene-enhanced quartz tuning fork for laser-induced thermoelastic spectroscopy," IEEE Sens. J. **21**, 9819 (2021).
48. Y. Pan, J. Zhao, P. Lu, C. Sima, W. Zhang, L. Fu, D. Liu, J. Zhang, H. Wu, and L. Dong, "All-optical light-induced thermoacoustic spectroscopy for remote and non-contact gas sensing," Photoacoustics **27**, 100389 (2022).
49. X. Liu, S. Qiao, G. Han, J. Liang, and Y. Ma, "Highly sensitive HF detection based on absorption enhanced light-induced thermoelastic spectroscopy with a quartz tuning fork of receive and shallow neural network fitting," Photoacoustics **28**, 100422 (2022).
50. L. Hu, C. Zheng, Y. Zhang, J. Zheng, Y. Wang, and F. K. Tittel, "Compact all-fiber light-induced thermoelastic spectroscopy for gas sensing," Opt. Lett. **45**, 1894 (2020).
51. A. Zifarelli, A. Sampaolo, P. Patimisco, M. Giglio, M. Gonzalez, H. Wu, L. Dong, and V. Spagnolo, "Methane and ethane detection from natural gas level down to trace concentrations using a compact mid-IR LITES sensor based on univariate calibration," Photoacoustics **29**, 100448 (2023).
52. Y. He, Y. Ma, Y. Tong, X. Yu, and F. K. Tittel, "Ultra-high sensitive light-induced thermoelastic spectroscopy sensor with a high Q-factor quartz tuning fork and a multipass cell," Opt. Lett. **44**, 1904 (2019).
53. Y. Ma, T. Liang, S. Qiao, X. Liu, and Z. Lang, "Highly sensitive and fast hydrogen detection based on light-induced thermoelastic spectroscopy," Ultrafast Sci. **3**, 0024 (2023).
54. X. Liu, and Y. Ma, "Sensitive carbon monoxide detection based on light-induced thermoelastic spectroscopy with a fiber-coupled multipass cell [Invited]," Chin. Opt. Lett. **20**, 031201 (2022).
55. S. Dello Russo, A. Zifarelli, P. Patimisco, A. Sampaolo,

T. Wei, H. Wu, L. Dong, and V. Spagnolo, "Light-induced thermo-elastic effect in quartz tuning forks exploited as a photodetector in gas absorption spectroscopy," Opt. Express **28**, 19074 (2020).

56. Y. Ma, S. Qiao, P. Patimisco, A. Sampaolo, Y. Wang, F. K. Tittel, and V. Spagnolo, "In-plane quartz-enhanced photoacoustic spectroscopy," Appl. Phys. Lett. **116**, 061101 (2020).
57. P. Patimisco, S. Borri, A. Sampaolo, H. E. Beere, D. A. Ritchie, M. S. Vitiello, G. Scamarcio, and V. Spagnolo, "A quartz enhanced photo-acoustic gas sensor based on a custom tuning fork and a terahertz quantum cascade laser," Analyst **139**, 2079 (2014).
58. F. Sgobba, A. Sampaolo, P. Patimisco, M. Giglio, G. Menduni, A. C. Ranieri, C. Hoelzl, H. Rossmadl, C. Brehm, V. Mackowiak, D. Assante, E. Ranieri, and V. Spagnolo, "Compact and portable quartz-enhanced photoacoustic spectroscopy sensor for carbon monoxide environmental monitoring in urban areas," Photoacoustics **25**, 100318 (2022).
59. C. Fang, S. Qiao, Y. He, Z. Shen, and Y. Ma, "Design and sensing performance of T-shaped quartz tuning forks," Acta Opt. Sin. **43**, 1899910 (2023).
60. Y. Liu and Y. Ma, "Advances in multipass cell for absorption spectroscopy- based trace gas sensing technology [Invited]," Chin. Opt. Lett. **21**, 033001 (2023).
61. Y. Liu, H. Lin, B. Montano, W. Zhu, Y. Zhong, R. Kan, B. Yuan, J. Yu, M. Shao, H. Dan, "Integrated near-infrared QEPAS sensor based on a 28 kHz quartz tuning fork for online monitoring of CO_2 in the greenhouse," Photoacoustics, **25**, 100332 (2022).
62. F. Chen, S, Jiang, H, Ho, S. Gao, Y. Wang, W. Jin, "Frequency-division-multiplexed multicomponent gas sensing with photothermal spectroscopy and a single NIR/MIR fiber-optic gas cell," Anal. Chem. **94**, 13473 (2022).